

Complexity growth rate during phase transitions

Mahdis Ghodrati

*Center for Gravitation and Cosmology, College of Physical Science and Technology,
Yangzhou University, Yangzhou 225009, China*

E-mail: ghodrati@umich.edu

Abstract

We present evidences for the connection between the potential of different fields and complexity growth rates both in conformal and confining cases. By studying different models, we also establish a strong connection between phase transitions and the discontinuities in the complexity growth rates. In the first example, for the dyonic black holes which are dual to van der Waals fluids, we find a similar first order phase transition in the behavior of complexity growth rate. We then compare the Schwinger effect and also the behavior of complexity in the AdS and AdS soliton backgrounds and comment on the connection between them. Finally, in a general Gubser model of QCD, we present the connections between the potentials, entropies, speed of sounds and complexity growth rates during crossover, first and second order phase transitions and also the behavior of quasinormal modes.

Contents

1	Introduction	1
2	The relationship between field potentials and complexity growth rates	3
2.1	Charged dilaton black hole in AdS space	3
2.2	Born-Infeld black hole in AdS Space	6
2.3	Charged black hole with phantom Maxwell field	7
3	Phase transitions and complexity growth rate with charge or kink	8
3.1	Complexity in dyonic black holes	8
3.2	Complexity and fluctuations in AdS soliton background	12
4	Complexity and phase transitions in QCD models	15
4.1	V_{QCD}	24
4.2	V_1	25
4.3	V_2	26
4.4	V_{IHQCD}	26
5	Discussion	28
	References	30

1 Introduction

In addition to Ryu-Takayanagi formula [1] which built a connection between the entanglement entropy as a quantum information quantity in the boundary, and the area of a codimension-two hypersurface, as a geometric quantity in the bulk, recently holographic quantum complexity [2–4] has been proposed which builds another connection between quantum information and geometry.

In the quantum information side, complexity would be the number of gates needed to go from one specific quantum state to another one and therefore, it quantifies how difficult a computational task would be. In the geometrical side, it could be calculated from the volume of a codimension-one surface which extends between two boundaries (complexity=volume, CV conjecture) or the action on the Wheeler-DeWitt patch (complexity=action, CA conjecture) [3, 5]. These conjectures have been studied extensively recently, see [6–26] for some examples.

In order to make this new connection more precise and use it in the holographic context, a more exact definition of complexity for the field theories are needed. The initial attempts were for the free scalar fields [27, 28], simple fermionic fields [29–31], and recently coherent [32] and simple interacting QFTs [33]. Generally there would be some ambiguities in defining the specific gates needed for each case.

In this work, first, we examine if there exist a relationship between quantum fluctuations of the system in different models, for instance between particle pair creations and annihilation rates, and the rates of growth of complexity. There are actually several reasons one might conjecture that such a connection between them exists. One reason is that the only physical process that still would occur even after the thermal equilibrium is just the quantum fluctuations which could be the main source of increasing the complexity. Also, it has been found that the complexity growth rate of black holes and also the worldsheet of a string dual to entangled particle-antiparticle would both saturate the Lyapunov bound [34]. Also, generally increasing the energy of the system would increase complexity growth rate.

To further examine this idea, in section 2, we study the potential wells and barriers of different fields in different models and also the complexity growth rates in them and in fact we observe such a relationship.

To learn more about the nature of holographic complexity, one could study its behavior in more exotic cases [35–43] such as various phase transitions and then try to establish the connections with other physical quantities of the system. This quest is the main purpose of this work.

In [36], the complexity in an interesting QCD model has been studied and the similarities between the first, second and crossover phase transitions both in entropy and complexity growth rate have been observed. Therefore, in that work, it has been shown that complexity could in fact act as a probe of different phase transitions and specially could probe the confinement. Also, in [40], using models of quantum harmonic oscillators, it has been shown that complexity can act as a probe of quantum quenches and can even capture features that entanglement entropy is not capable of probing. Along the works of those papers, we would like to study the complexity growth rates in various phase transition setups.

Therefore, first, in section 3.1, we study charged dyonic black hole model which are the system which could mimic the properties of van der Waals fluid, and already using the Gibbs free energy, the first and second order phase transitions have been observed in them. Using the full time dependent complexity growth rate, we also observe phase transition in the complexity growth rate of this model.

Then in section 3.2, we consider AdS and AdS soliton backgrounds, study their potentials, the complexity growth rate in each background and examine the connection between the phase transitions such as tachyon condensation and complexity growth rate behaviors specifically in the IR and UV regions and again illustrate the connection. We also compare the Schwinger effect phase diagrams in these two cases and comment on the relationship with the complexity.

Finally, in section 4, we study the phase transitions in the Gubser model of QCD. In this model, by just fine tuning the parameters of the confining potential, in the diagram of entropy versus temperature, one could obtain crossover, first and second order first transitions for the V_{QCD} , V_1 and V_2 respectively. Also, we study another model of improved holographic QCD, V_{IHQCD} , which could present a first order phase transition while give a more effective model for the dynamical

properties of QCD such as asymptotic freedom and a more realistic bulk viscosity. This model shows substantial differences in the behavior of quasinormal modes and also complexity, which we will discuss in details.

Therefore, we study the behavior of entropy, complexity growth rate, speed of sound and potential for all these four models and compare the behavior of them at lower temperatures and specifically near the phase transitions. We also outline the relationship between the cross over from hydrodynamic to non-hydrodynamic modes of each model, and the resulting topological jump in the complexity growth rate around the phase transition point.

Finally, we conclude with a discussion in section 5.

2 The relationship between field potentials and complexity growth rates

By comparing the results for the complexity growth rates in different black hole solutions with different fields, in this section, we study the connections between action growth rates and then the dilaton field, Maxwell field, electric and magnetic fields of black hole solutions. So in this section we first review the already calculated results for different backgrounds which have fields with different natures, and then we discuss the connection between the behavior of their potentials and the complexity growth rates.

2.1 Charged dilaton black hole in AdS space

First, we consider the Einstein-Maxwell-dilaton model [6]

$$S = \frac{1}{16\pi} \int d^4x \sqrt{-g} (R - 2(\partial\phi)^2 - V(\phi) - e^{-2\phi} F^2), \quad (2.1)$$

where the potential $V(\phi)$ for the dilaton field is

$$V(\phi) = -\frac{4}{l^2} - \frac{1}{l^2} [e^{2(\phi-\phi_0)} + e^{-2(\phi-\phi_0)}]. \quad (2.2)$$

Here ϕ_0 is a constant and l is the AdS radius. So, this potential is the combination of a constant value and two Liouville-type potentials. The spherically symmetric charged dilaton black hole solution of this action would be

$$\begin{aligned} ds^2 &= -f(r)dt^2 + f^{-1}(r)dr^2 + U^2(r)d\Omega^2, \\ F_{rt} &= \frac{Qe^{2\phi}}{U^2}, \quad e^{2\phi} = e^{2\phi_0} \left(1 - \frac{2D}{r}\right), \end{aligned} \quad (2.3)$$

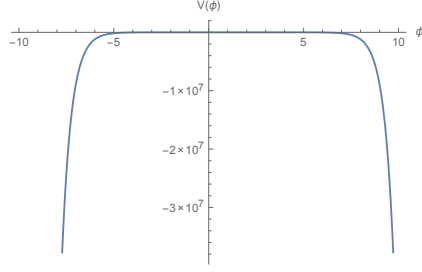


Figure 1: Two Liouville-type potential 2.2

where

$$f(r) = 1 - \frac{2M}{r} + \frac{r(r - 2D)}{l^2}, \quad U^2(r) = r(r - 2D), \quad D = \frac{Q^2 e^{2\phi_0}}{2M}. \quad (2.4)$$

In [6], for the charged dilaton AdS black hole, the complexity has been found as

$$\text{charged dilation AdS BH : } \frac{dS}{dt} = 2M - \mu_+ Q - D, \quad D = \frac{Q^2 e^{2\phi_0}}{2M}, \quad (2.5)$$

where D is the dilaton charge and ϕ_0 is the asymptotic constant value of dilaton [44]. Note that when $\phi = \phi_0 = 0$, this solution reduces to the Reissner-Nordstrom black hole.

By plotting \dot{C} versus ϕ_0 and r , and by comparing it with the behavior of the dilaton potential $V(\phi)$ and also Maxwell field $F(\phi)$, one could notice some interesting correlations.

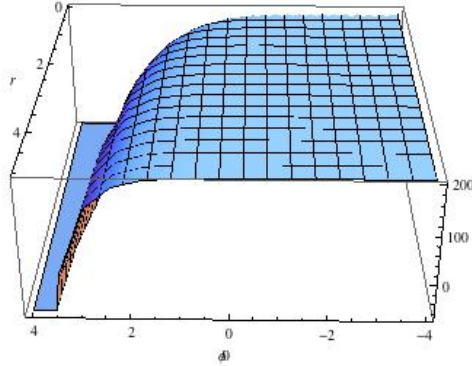


Figure 2: The plot of $\frac{dS}{dt}$ or complexity growth rate for charged dilaton black hole.

From figure 2, one can notice that for the negative ϕ_0 , with large absolute values, the complexity is constant, then at a specific positive value of ϕ_0 , it decreases exponentially. Therefore, as a first observation, one could say that generally by increasing the dilaton field, the complexity growth rate would decrease.

Recently in [45], the effect of dilaton field on the complexity growth rate has been studied further where the *full time* behavior of the action growth rate for the AdS dilaton black hole and also asymptotically Lifshitz black holes have been studied. Generally as it was shown in [45] with another method, the dilaton field would actually slow down the rate of growth of complexity

which we observed here as well. In section 4, the same result would be seen in models of confining potentials, so we conjecture it would be a universal effect.

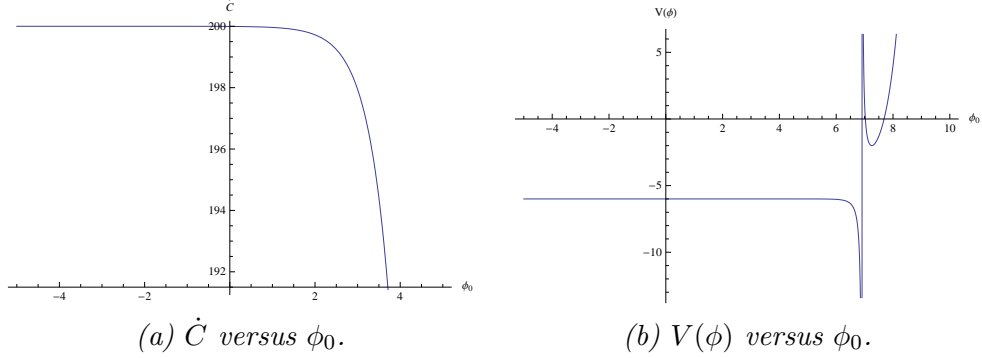


Figure 3: Comparison between the complexity growth rate and potential in the charged dilaton black hole.

The comparison between the potential behavior of the dilaton and complexity growth rate is then shown in Fig. 3. So for the small and also negative ϕ_0 , the dilaton potential is constant, then there is a barrier at a positive value of ϕ_0 and then the potential barrier increases exponentially. When there is a big barrier in the potential, the rate of growth of complexity falls down exponentially and eventually becomes zero. On the other hand, when the potential is constant, the complexity growth rate \dot{C} would remain constant as well. We will see the same kind of behavior in the QCD models. So again this could point out to a relationship between quantum fluctuations produced by the dilaton potential and the complexity growth rate.

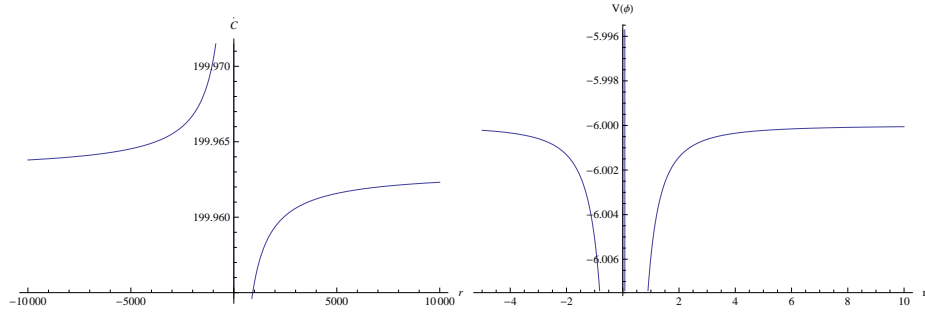


Figure 4: Behavior of \dot{C} and $V(\phi)$ vs. r for charged dilaton black hole.

From Fig. 4, once again the similarities between the potential behavior and the complexity growth rate could be observed, as in the large r , both the potential and also the complexity growth rate become constant. Also, in small values of r , there is a potential well and for those values the complexity growth rate becomes very small too. This again could indicate a connection between quantum fluctuations such as tunneling or pair creation and complexity growth rate.

The same result could be deduced by comparing plots of the Maxwell field, $F(\phi)$. As can be seen from 5, for large ϕ_0 , $F(\phi)$ becomes zero which also makes complexity growth rate small and then zero at the end, hinting to the relationship between the two.

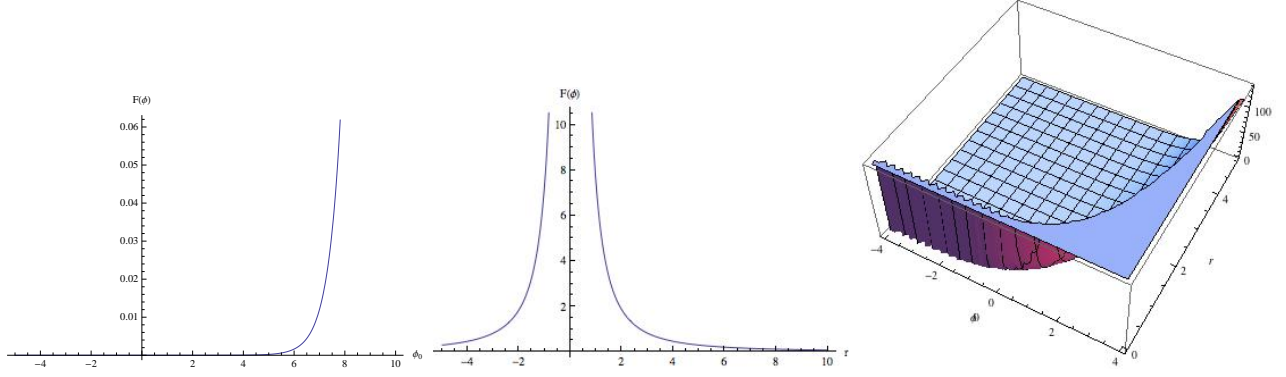


Figure 5: Behavior of Maxwell field, $F(\phi)$ vs. ϕ_0 and r .

2.2 Born-Infeld black hole in AdS Space

Another example of charged black hole in AdS is Born-Infeld, with the following action

$$S = \frac{1}{16\pi} \int d^4x \sqrt{-g} \left[R + \frac{6}{l^2} + 4\beta^2 \left(1 - \sqrt{1 + \frac{F_{\mu\nu}F^{\mu\nu}}{2\beta^2}} \right) \right], \quad (2.6)$$

where one can get a static symmetrically symmetric black hole solution as follows

$$ds^2 = -f(r)dt^2 + f^{-1}(r)dr^2 + r^2d\Omega^2, \quad F_{rt} = \frac{Q}{\sqrt{r^4 + Q^2/\beta^2}}, \quad (2.7)$$

where

$$\begin{aligned} f(r) &= 1 - \frac{2M}{r} + \frac{r^2}{l^2} + \frac{2\beta^2}{r} \int_r^\infty dx \left(\sqrt{x^4 + Q^2/\beta^2} - x^2 \right) \\ &= 1 - \frac{2M}{r} + \frac{r^2}{l^2} + \frac{2\beta^2}{r} \left[I(r = \infty; a^2 = \frac{Q^2}{\beta^2}) - I(r; a^2 = \frac{Q^2}{\beta^2}) \right], \end{aligned} \quad (2.8)$$

and $I(r; a^2) \equiv \int_r^\infty dx (\sqrt{x^4 + a^2} - x^2)$.

Here M and Q , are the mass and charge of the black hole. Also note when $\beta \rightarrow \infty$, the Born-Infeld theory reduces to the Maxwell theory with $\mathcal{L}(F) = -F^2$. The chemical potential of this black hole could also be obtained as

$$\mu(r)Q = \frac{Q^2}{r} {}_2F_1\left[\frac{1}{4}, \frac{1}{2}, \frac{5}{4}, -\frac{Q^2}{\beta^2 r^4}\right]. \quad (2.9)$$

As found in [6] when $\beta^2 Q^2 \geq 1/4$ the black hole solution has two horizons and when $\beta^2 Q^2 < 1/4$, it has only one horizon where the inner one is absent. So changing the coupling β or the charge Q could greatly impact the complexity as it significantly changes the geometry.

For the case with two horizons, [6] found the action growth as

$$\frac{dS}{dt} = \mu_- Q - \mu_+ Q. \quad (2.10)$$

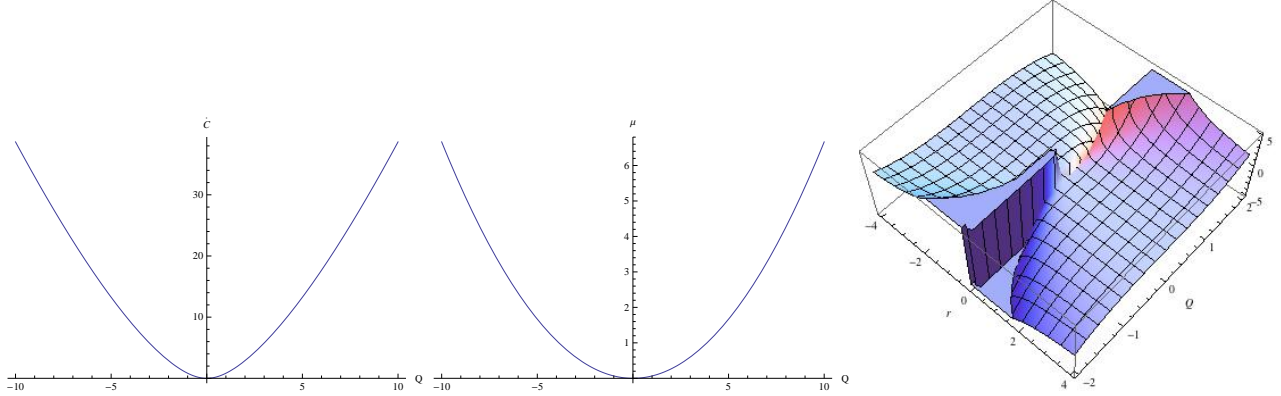


Figure 6: Behavior of complexity growth and chemical potential vs. Q for the Born-Infeld black hole.

In figure 6, the relationships between complexity growth, charge and chemical potential have been studied. One can see that generally increasing the charge of the black hole Q , would increase the rate of growth of complexity. Obviously as increasing the charge could intensify the vacuum quantum fluctuations, this solution once more shows our conjectured connection.

In figure 6 note that $r = 0$ is a spacelike singularity, which makes the behavior of complexity growth rate discontinuous there.

2.3 Charged black hole with phantom Maxwell field

As another example, we consider the action of Einstein-phantom-Maxwell theory with a negative cosmological constant as

$$S = \frac{1}{16\pi} \int d^4x \sqrt{-g} (R + \frac{6}{l^2} + F_{\mu\nu} F^{\mu\nu}), \quad (2.11)$$

where its solution would be

$$ds^2 = -f(r)dt^2 + f^{-1}(r)dr^2 + r^2 d\Omega^2, \quad F_{tr} = \frac{Q}{r^2}, \quad f(r) = 1 + \frac{r^2}{l^2} - \frac{2M}{r} - \frac{Q^2}{r^2}. \quad (2.12)$$

Its Penrose diagram is the same as AdS Schwarzschild black hole. The action growth rate has been found as $\frac{dS}{dt} = 2M + \mu_+ Q$.

Again, one can see from 7, increasing Q increases the complexity growth rate as it increases the quantum fluctuations, similar to the result we found before. Note that this connection holds even though the phantom Maxwell field does not satisfy the energy condition and as the result the Lloyd's bound.

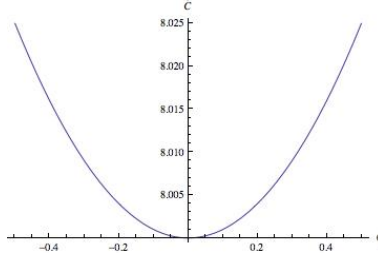


Figure 7: \dot{C} vs. Q for the phantom Maxwell field.

3 Phase transitions and complexity growth rate with charge or kink

We now study the full time behavior of complexity growth rate for the dyonic and AdS soliton black holes and compare them with their different phase transitions. We find that generally the complexity growth rate could probe any kind of phase transition and instability.

3.1 Complexity in dyonic black holes

First, we consider the dyonic black hole in the holographic setup similar to [46]. We chose this type of black hole as it has both electric and magnetic charges. It could be a solution to the Reissner-Nordstrom action with the negative cosmological constant,

$$I = \frac{1}{16\pi} \int d^d \sqrt{g} [\mathcal{R} - 2\Lambda - F^{\mu\nu} F_{\mu\nu}], \quad (3.1)$$

where the static spherically symmetric solution would be

$$ds^2 = -f(r)dt^2 + \frac{dr^2}{f(r)} + r^2 d\Omega^2, \quad f(r) = 1 - \frac{\Lambda r^2}{3} - \frac{2m}{r} + \frac{q_E^2 + q_M^2}{r^2},$$

$$A = \left(-\frac{q_E}{r} + \frac{q_E}{r_+} \right) dt + (q_M \cos \theta) d\phi. \quad (3.2)$$

The charge and mass of this solution are

$$M = \frac{2\Omega_2}{16\pi} \left(r_+ + r_- + \frac{1}{l^2} \frac{r_+^4 - r_-^4}{r_+ - r_-} \right), \quad Q^2 = \frac{2\Omega_2}{8\pi} r_+ r_- \left(1 + \frac{1}{l^2} \frac{r_+^3 - r_-^3}{r_+ - r_-} \right), \quad (3.3)$$

and the chemical potentials would be $\mu_- = Q/r_-$, $\mu_+ = Q/r_+$ and also $Q^2 = q_M^2 + q_E^2$.

The complexity growth rate for this solution *at late times* has been found as [21]

$$\frac{dS_{bk+bd}}{dt} = (M - \mu_+ Q) - (M - \mu_- Q). \quad (3.4)$$

Now we find the full, time dependent, holographic complexity. First, we divide the bulk action

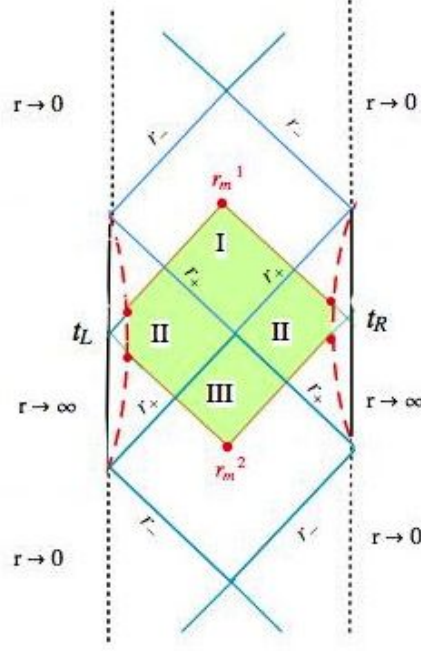


Figure 8: Penrose diagram of the dyonic charged black hole. The Wheeler-DeWitt patch is shown in green.

as

$$\begin{aligned}
I_I^{\text{bulk}} &= \frac{\Omega_2}{8\pi G_N} \int_{r_+}^{r_{\text{max}}} dr \left[-\frac{2r^3}{l^2} - \frac{2r_+r_-}{r} \left(1 + \frac{1}{l^2} \frac{r_+^3 - r_-^3}{r_+ - r_-} \right) \right] \left(\frac{t}{2} + r^*(0) - r^*(r) \right), \\
I_{II}^{\text{bulk}} &= \frac{\Omega_2}{4\pi G_N} \int_{r_-}^{r_+} dr \left[-\frac{2r^3}{l^2} - \frac{2r_+r_-}{r} \left(1 + \frac{1}{l^2} \frac{r_+^3 - r_-^3}{r_+ - r_-} \right) \right] (r^*(0) - r^*(r)), \\
I_{III}^{\text{bulk}} &= \frac{\Omega_2}{8\pi G_N} \int_{r_+}^{r_m} dr \left[-\frac{2r^3}{l^2} - \frac{2r_+r_-}{r} \left(1 + \frac{1}{l^2} \frac{r_+^3 - r_-^3}{r_+ - r_-} \right) \right] \left(\frac{-t}{2} + r^*(0) - r^*(r) \right).
\end{aligned}$$

The sum of these terms would be

$$\begin{aligned}
I^{\text{bulk}} &= \frac{\Omega_2}{8\pi G_N} \int_{r_m}^{r_{\text{max}}} dr \left[-\frac{2r^3}{l^2} - \frac{2r_+r_-}{r} \left(1 + \frac{1}{l^2} \frac{r_+^3 - r_-^3}{r_+ - r_-} \right) \right] \left(\frac{t}{2} - r^*(0) + r^*(r) \right), \\
&+ \frac{\Omega_2}{4\pi G_N} \int_{r_-}^{r_{\text{max}}} dr \left[-\frac{2r^3}{l^2} - \frac{2r_+r_-}{r} \left(1 + \frac{1}{l^2} \frac{r_+^3 - r_-^3}{r_+ - r_-} \right) \right] (r^*(0) - r^*(r)),
\end{aligned}$$

By choosing the following normal vectors,

$$k_1^a = \alpha \left(\frac{1}{f(r)} (\partial_t)^a + (\partial_r)^a \right), \quad k_2^a = \beta \left(-\frac{1}{f(r)} (\partial_t)^a + (\partial_r)^a \right), \quad (3.5)$$

and the joint action

$$I^{\text{joint}} = \frac{1}{8\pi G_N} \int d^d x \sqrt{\gamma} \log \left| \frac{k_1 \cdot k_2}{2} \right|, \quad (3.6)$$

the contribution from this term at $r = r_m$ would then be found as

$$I^{\text{joint}} = \frac{\Omega_2}{8\pi G_N} r_m^2 \log \left| \frac{\alpha\beta}{f(r_m)} \right|. \quad (3.7)$$

Also, for the counter term,

$$\frac{1}{8\pi G_N} \int d\lambda d^d x \sqrt{\gamma} \log \frac{\Theta}{d}, \quad (3.8)$$

we find

$$\Theta = \frac{1}{\sqrt{\gamma}} \frac{\partial \sqrt{\gamma}}{\partial \lambda} = \frac{2\alpha}{r}. \quad (3.9)$$

Here, λ is the affine parameter for the null surface. For the null vector k_1 it would be

$$\frac{\partial r}{\partial \lambda} = \alpha, \quad (3.10)$$

So finally we get

$$I^{ct} = \frac{\Omega_2}{8\pi G_N} r_m^2 \log |\alpha\beta| + \frac{\Omega_2}{8\pi G_N} (r_m^2 - 2r_m^2 \log r_m), \quad (3.11)$$

where the first term can eliminate the ambiguity coming from the normalization factors of the null vectors. Summing all of these terms, taking the time derivative, removing some remaining constant terms, and using $\frac{dr_m}{dt} = -\frac{f(r_m)}{2}$, we finally get the relationship

$$\frac{d}{dt} \mathcal{C} \propto -\frac{f(r_m) r_m^3}{16} (1 + 4 \log r_m) + f(r_m) r_m \log \left(\frac{f(r_m)}{r_m^2} \right) + \frac{r_m^2 f'(r_m)}{2}. \quad (3.12)$$

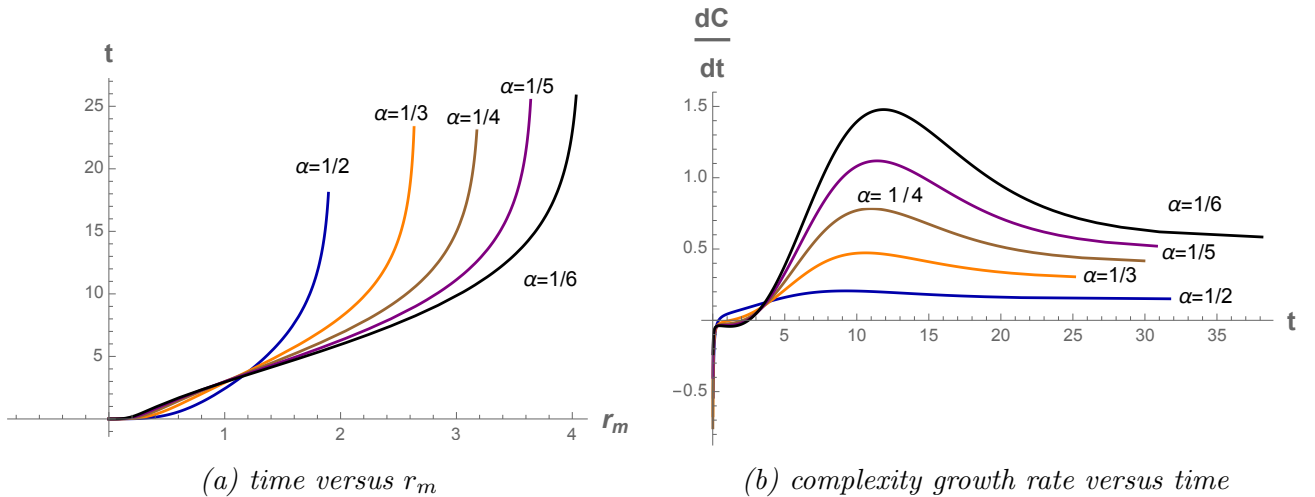


Figure 9: The full time behavior of complexity growth rate of dyonic black holes.

The plots for the behavior of complexity of dyonic black holes are shown in Fig 9b where α is just a constant we chose which is defined as $\Lambda = m = q_E = q_M = \alpha$.

From these diagrams, one can see that the Lloyd's bound at early times would be violated and at later times it would be saturated from above similar to other studies in [8, 43, 47, 48].

In addition, we could notice that by increasing the electric and magnetic charges, q_E , q_M , the maximum of $\frac{dC}{dt}$ would increase and therefore the violation of Lloyd's bound at early times would become stronger. Also, the limit of Lloyd's bound at late times would increase as well. Note that this again could point to a relationship between quantum fluctuations like Schwinger mechanism and the complexity growth rate as we have conjectured before. Of course to further study this relation, one could study the Schwinger effect for other charged black holes with varied setups of gauge fields. For instance, the electric and magnetic fields might have different directions with respect to each other and then one could study the complexity growth rate for those varied angle setups, and therefore further quantify this connection.

Additionally, from these diagrams, one could notice that, keeping the charges constant while increasing m or Λ would decrease the maximums in the plots of $\frac{dC}{dt}$ versus t , and also its final late time limit which is the Lloyd's bound. It would also decrease the time which is needed to reach to that specific Lloyd's bound.

By keeping m and Λ constant and changing q_E and q_M , one can observe different phases which are shown in the plots of $\frac{dC}{dt}$ versus time in Fig. 10.

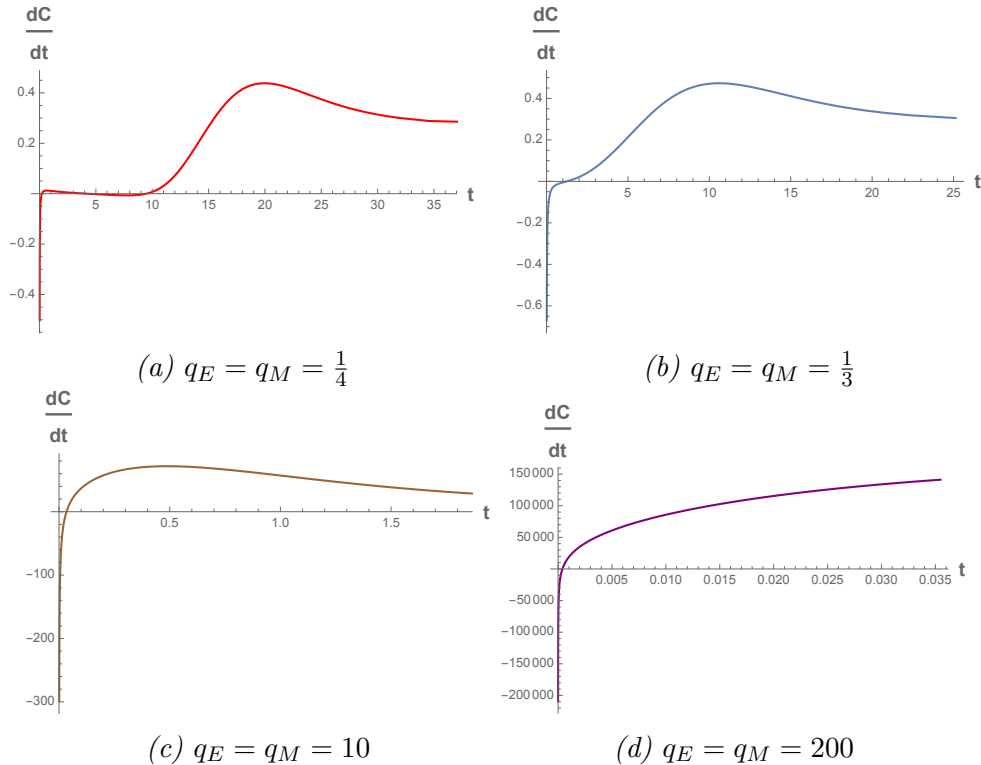


Figure 10: The change of behavior in complexity growth rate by changing the charges of dyonic black holes.

One could notice that for very small charges, the complexity growth rates at the beginning are very close to zero and only fluctuate a little bit at the early times, then suddenly increase and reach to their maximum and finally at the later times approach the corresponding Lloyd's bound, Fig. 10a.

Increasing the charges would smooth out the fluctuations at the beginning and make the rate of complexity growth to reach to its maximum and then its Lloyd's bound much faster which could be noticed from the time axis of Figs 10b, 10c.

For very large charges, the complexity growth rate would diverge. This could only mean that the dyonic black hole is unstable for those ranges of charge, see Fig. 10d. So, in addition to the various phase transitions, complexity growth rate could even capture the instabilities in the solution of black holes.

One could also consider some additional counter terms for these dyonic black holes similar to [43], and consider their effects. This might solve the peculiar behavior at the beginning of our diagrams or it might even solve the issue of violation of Lloyd's bound at the early times.

Note that as the dyonic black holes are the dual holographic model for the van der Waals fluids [46, 49, 50], we expect that the behavior of complexity growth rate for these systems would just be similar to the diagrams in 9b and this could probably be tested in the lab.

3.2 Complexity and fluctuations in AdS soliton background

Now in this section we study the AdS soliton solution which is a confining geometry but still is very similar to the conformal AdS case as it could be transformed to it by a double Wick rotation.

The AdS soliton background is

$$ds^2 = \frac{r^2}{\ell^2} \left[-dt^2 + \left(1 - \frac{r_+^d}{r^d} \right) d\chi^2 + d\vec{x}^2 \right] + \left(1 - \frac{r_+^d}{r^d} \right)^{-1} \frac{\ell^2}{r^2} dr^2, \quad (3.13)$$

where χ is the circle with anti periodic boundary conditions.

This solution has the following negative boundary energy [31],

$$E = -\frac{r_+^d \Delta \chi V_x}{\ell^{d+1}}. \quad (3.14)$$

This ground state energy is the result of variance between the Casimir energies of bosons and fermions which exists due to the anti periodic boundary conditions for the fermions. Increasing the anti periodicity would increase this negative Casimir energy and as a result the complexity.

In [51], it has been shown that there is a connection between AdS bubbles (AdS solitons) and closed string tachyon condensations, and also it has been found in that work, that the degrees of freedom and therefore the entanglement entropy would decrease under this tachyon condensation, (which is a second order phase transition). Also the energy density would decrease in this process

[52,53] and consequently the complexity would also decrease.

By considering the gates with penalty factors which could take into account the entanglement between such gates, one could check the reduction of complexity during this process from the field theory side. Doing that would probably end up with a different result from the one [31], so then their calculation of complexity from CV conjecture would match with the result of the field theory calculations.

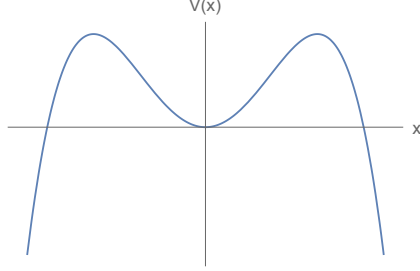


Figure 11: The effective tachyon potential for the p -adic string, $p > 2$. [54]

In [31] actually using both holographic CV and CA conjectures, the complexity for the background of AdS soliton has been calculated. Specifically, using CA conjecture, the authors in [31], calculated the full IR/UV behavior of complexity growth rate. They have found that by increasing the IR scale, the action first increases until reaching a maximum and then it would decrease to zero at the UV cutoff. We reproduce the plot for the whole action versus the radial distance for the case of AdS soliton in Fig. 12. This actually comes from Eq. 38 of [31], where all the boundary and joint terms have been considered.

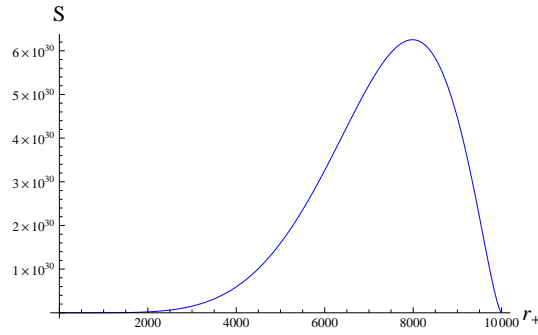


Figure 12: S v.s r_+ .

Comparing the behavior of complexity, potentials, (see figures 11 and 12), and also the phase diagrams of Schwinger pair creation in two backgrounds of AdS and AdS soliton,(see Fig. 13), could again point out to a relationship between computational complexity and the vacuum fluctuations. One could again see that the bigger potential barriers generally decrease the complexity and its growth rate.

Using the CV conjecture, the complexity in AdS soliton has been found as [31]

$$\mathcal{C}_V = \frac{8V_x \Delta \chi}{\pi} \frac{r_{max}^{d-1} - r_+^{d-1}}{\ell^{d-1}} \quad (3.15)$$

where V_x is just the IR divergent volume in the x direction and the first term is the complexity of AdS case. Therefore, one could see that the complexity of AdS soliton case is smaller than the AdS case which sounds a reasonable result. Note that, relative to the AdS soliton, pure AdS is the excited state and therefore as its energy is higher, one would expect the complexity of AdS would also be higher than AdS soliton background.

To get further information, one could compare the phase diagrams of Schwinger effect in both AdS and AdS soliton backgrounds while an electric field is present, see Fig. 13.

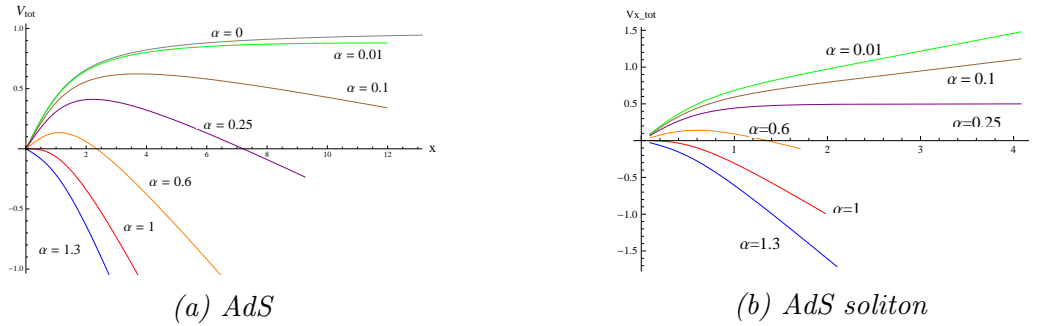


Figure 13: Comparing Schwinger phase diagrams of AdS and AdS soliton case.

At each value for alpha which here is the dimensionless quantity for the strength of electric field, i.e, $\alpha = \frac{E}{E_c}$, the potential of AdS soliton would be higher, pointing to smaller fluctuations and therefore smaller complexity. There are also three phases in the AdS soliton background while there are two phases for the AdS case. This richer possibilities for the phases could also be seen from the behavior of complexity.

Also in [55], the quasinormal modes in the AdS soliton case has been plotted. One could notice that for higher radial distances, these modes exponentially damp which explains the vanishing of complexity there.

This connection could be examined further in future works. For instance one could then turn on a magnetic field in addition to the electric field and change the angle between the direction of the two which could change the Schwinger pair creation rate greatly. As a universal result, [56] found that when the electric field is parallel to the electric field the pair creation rate is higher relative to the setup where they are perpendicular to each other. The complexity growth rates in these two setups would also be different. The results could be compared with the pair creation rates so to find more evidences for our conjecture of connection between quantum fluctuations and complexity growth rate.

4 Complexity and phase transitions in QCD models

To further study the relationship between potentials, quantum fluctuations, phase transitions and complexity growth, we study the Gubser model of QCD [57–61], as the main part of this work.

By tuning the parameters of the potential, in this model several kinds of phase transitions could be displayed. Based on the parameters of the dilaton potential, it could generate three types of phase transitions which are crossover, first and second order. We study the full time behavior of complexity growth rates around these phase transitions and the correlations with other thermodynamical quantities.

In [36], by using the CA conjecture, the late-time behavior of complexity of this holographic QCD model has been studied. There, it has been shown that the growth rate of complexity could also be used as a parameter to detect the phase transitions. This is because the behavior of entropy and complexity growth rate versus temperature would match up for each type of phase transition. We then study the connection between the behavior of complexity growth rates, speed of sound, entropy and potential for four different models of confining potentials.

The action of this model is

$$S = \frac{1}{16\pi G_5} \int d^5x \sqrt{-g} \left[R - \frac{1}{2}(\partial\phi)^2 - V(\phi) \right] + \frac{1}{8\pi G_5} \int_{\partial\mathcal{M}} K, \quad (4.1)$$

where K is the trace of the extrinsic curvature. For simplicity we also take $16\pi G_5 = 1$ and $\hbar = 1$.

In this model the five-dimensional gravity is coupled to a single scalar field. This setup then contains the minimum freedom which is needed to match the equation of states and also reproduce the desired phase diagrams of QCD.

The general ansatz for the dilaton potential would be

$$V(\phi) = -12(1 + a \phi^2)^{1/4} \cosh(\gamma\phi) + b_2\phi^2 + b_4\phi^4 + b_6\phi^6, \quad (4.2)$$

where $(a, \gamma, b_2, b_4, b_6)$ are the parameters shown below.

potential	a	γ	b_2	b_4	b_6	Δ	T_c
V_{QCD}	0	0.606	1.4	-0.1	0.0034	3.55	0.181033
V_{2nd}	0	$1/\sqrt{2}$	1.958	0	0	3.38	0.243901
V_{1st}	0	$\sqrt{7/12}$	2.5	0	0	3.41	0.156841
V_{IHQCD}	1	$\sqrt{2/3}$	6.25	0	0	3.58	0.295847

To compare the behavior of potential, with their different parameters, which then would lead to various phase transitions, the plots of $V(\phi)$ and $\frac{\partial_\phi V}{V}$ versus ϕ is shown in Fig. 14. The parameters in this potential [57, 58, 62] have been chosen in a way that the plots of c_s^2 versus T/T_c would match with the phenomenological results of hadron gas and also the lattice models. We discuss the properties of each model at the later parts of this section.

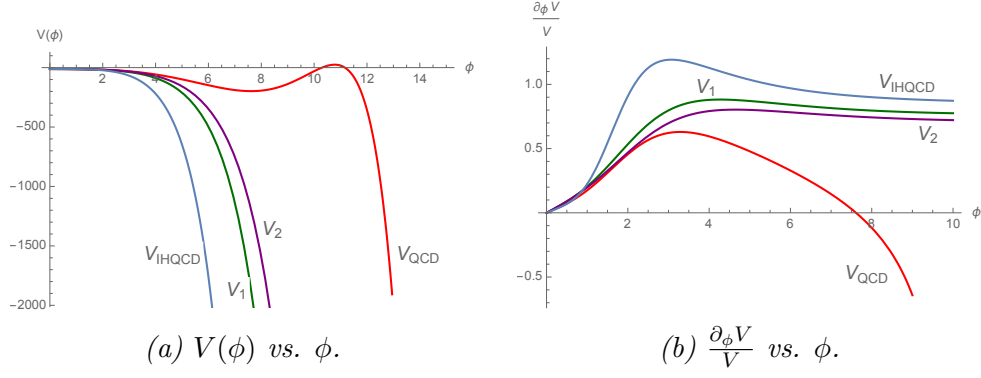


Figure 14: QCD potentials and their derivative vs. ϕ .

So first, we consider the following ansatz

$$ds^2 = e^{2A}(-h dt^2 + d\vec{x}^2) + \frac{e^{2B}}{h} dr^2, \quad \phi = r, \quad (4.3)$$

where A, B and h are only the functions of r (or ϕ). Note that the asymptotic boundary is at $r \rightarrow 0$ and the singularity is where $r \rightarrow \infty$.

The equations of motion would be

$$\begin{aligned} A'' - A'B' + \frac{1}{6} &= 0, \\ h'' + (4A' - B')h' &= 0, \\ 6A'h' + h(24A'^2 - 1) + 2e^{2B}V &= 0, \\ 4A' - B' + \frac{h'}{h} - \frac{e^{2B}}{h}V' &= 0, \end{aligned}$$

and the horizon is where $h(\phi_H) = 0$.

In [63], using the method of [57, 58], the field equations have been solved as

$$\begin{aligned} A(\phi) &= A_H + \int_{\phi_H}^{\phi} d\tilde{\phi} G(\tilde{\phi}), \\ B(\phi) &= B_H + \ln \left(\frac{G(\phi)}{G(\phi_H)} \right) + \int_{\phi_H}^{\phi} \frac{d\tilde{\phi}}{6G(\tilde{\phi})}, \\ h(\phi) &= h_H + h_1 \int_{\phi_H}^{\phi} d\tilde{\phi} e^{-4A(\tilde{\phi}) + B(\tilde{\phi})}, \end{aligned}$$

where $G(\phi) \equiv A'(\phi)$ and then using the initial and boundary conditions, the constants have been

found as

$$\begin{aligned}
A_H &= \frac{\ln \phi_H}{\Delta - 4} + \int_0^{\phi_H} d\phi \left[G(\phi) - \frac{1}{(\Delta - 4)\phi} \right], \\
B_H &= \ln \left(-\frac{4V(\phi_H)}{V(0)V'(\phi_H)} \right) + \int_0^{\phi_H} \frac{d\phi}{6G(\phi)}, \\
h_H &= 0, \\
h_1 &= \frac{1}{\int_{\phi_H}^0 d\phi e^{-4A(\phi)+B(\phi)}}.
\end{aligned}$$

For finding the solution of $G(\phi)$, one actually needs to solve the following equation

$$\frac{G'}{G + V/3V'} = \frac{d}{d\phi} \ln \left(\frac{G'}{G} + \frac{1}{6G} - 4G - \frac{G'}{G + V/3V'} \right), \quad (4.4)$$

and from it, one could find the series expansion of $G(\phi)$ near the horizon $\phi = \phi_H$ as

$$G(\phi) = -\frac{V(\phi)}{3V'(\phi)} + \frac{1}{6} \left(\frac{V(\phi_H)V''(\phi_H)}{V'(\phi_H)^2} - 1 \right) (\phi - \phi_H) + \mathcal{O}(\phi - \phi_H)^2. \quad (4.5)$$

This result could be used as the boundary condition for solving $G(\phi)$.

Assuming $16\pi G_5 = 1$ and $\hbar = 1$, the temperature, entropy and the speed of sound c_s , could be written as

$$T = \frac{e^{A_H - B_H}}{4\pi} |h'(\phi_H)| = \frac{e^{A_H + B_H}}{4\pi} |V'(\phi_H)|, \quad s = 4\pi e^{3A_H}, \quad c_s^2 = \frac{d \log T}{d \log s}. \quad (4.6)$$

Solving for these parameters numerically, the plots for the entropy and speed of sound versus temperature for the four models of potential could be constructed, which they are shown in Fig. 15 and Fig. 16. Note that in all of these models s/T^3 is actually proportional to the number of degrees of freedom [63]. Therefore, beforehand, one could expect that the behavior of complexity growth rate would be similar to entropy as well.

For the late-time interval $[t, t + \delta t]$, the bulk term of the on-shell action inside the horizon is

$$S_{\text{bulk}} = \int d^5x \frac{2}{3\pi G_N} e^{4A+B} V(r) = \frac{2V_3}{3\pi G_N} \int_t^{t+\delta t} dt \int_{r_H}^\infty e^{4A+B} V(r) dr, \quad (4.7)$$

and the GHY term would be

$$S_{\text{GHY}} = \delta t V_3 \left[e^{-4A-B} \partial_r (e^{8A} h) \right] \Big|_{r_H}^\infty, \quad (4.8)$$

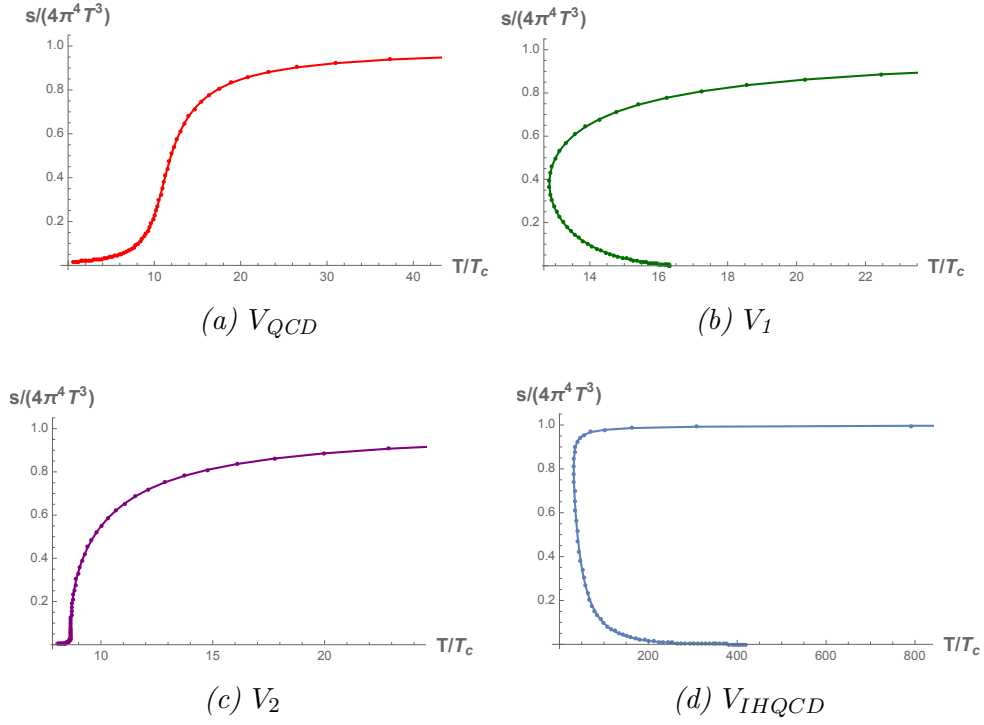


Figure 15: Phase transition of entropy versus temperature for four non-conformal cases.

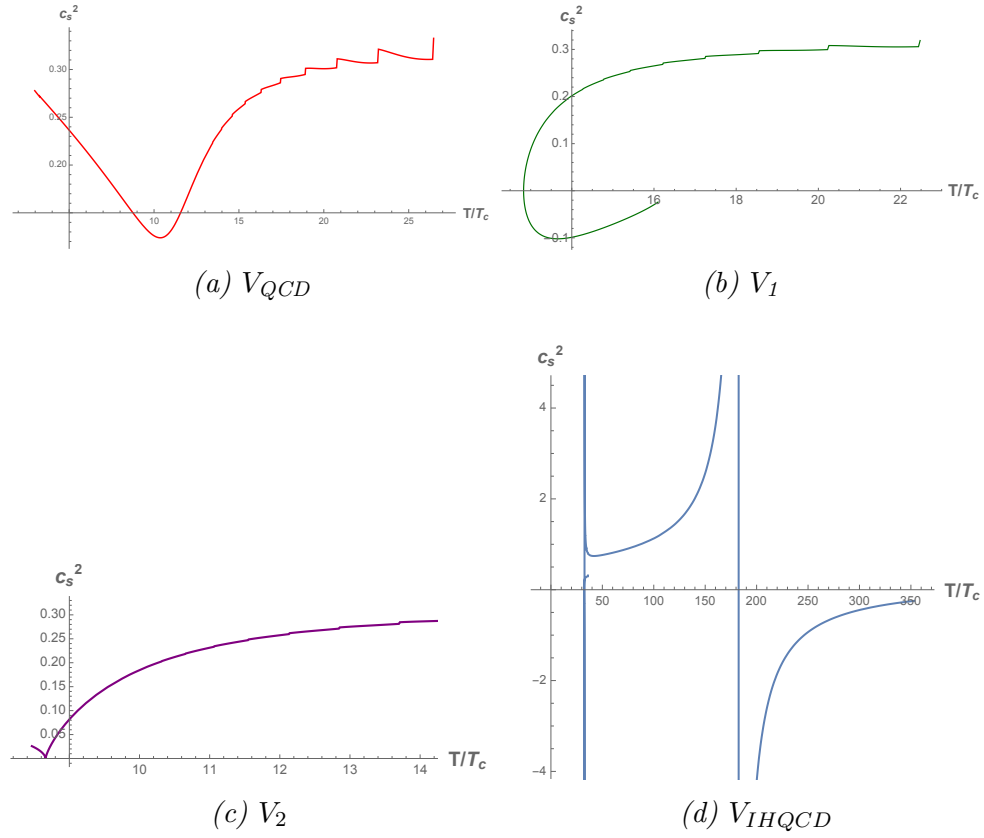


Figure 16: The diagrams of speed of sound versus T/T_c for four non-conformal cases.

where $V_3 \equiv \int d^3\vec{x}$ is the volume of the boundary field system.

So the growth rate of the holographic complexity density $c \equiv \mathcal{C}/V_3$ at late time is

$$\frac{dc}{dt} = \frac{2}{3\pi G_N} \int_{r_H}^{\infty} e^{4A+B} V(r) dr + \frac{1}{\pi} \left[e^{-4A-B} \partial_r (e^{8A} h) \right] \Big|_{r_H}^{\infty}. \quad (4.9)$$

The plots for the behavior of late time complexity during each phase transition are presented in Fig. 17. As one would expect and as found in [36] they are very similar to the diagrams of entropy for each potential, demonstrating that complexity could also act as a good probe of confinement and phase transitions.

Interestingly the jump that we see in the complexity for all of these cases during the phase transition is close to the topological jump of $\Delta\mathcal{C} = 2\pi$ found in [12, 26]. So it is worth noting that the results in here coming from the “complexity=action” conjecture is fairly consistent with the results of [12] which has come from the “complexity=volume” and the “subregion complexity” conjectures, [4, 5, 64, 65].

Comparing these diagrams with those of the speed of sound [66] would be interesting too. Note that for the high temperatures where the first three models become conformal, the speed of sound becomes constant and close to 0.3 and also the rate of complexity growth would become constant as well. For the low temperature case, note that when the slope of diagrams for the c_s^2 versus T/T_c is negative, the slope of c_s^2 versus T/T_c would be positive and vice versa. This qualitatively could be explained by the fact that when the speed of sound grows in a region, the information could propagate easier, it would be easier to go from one state to another and therefore, the rate of growth of complexity would decrease.

Now we study the full time behavior of complexity growth rate in this model. Similar to [8, 67], the time evolution of complexity could be found by adding the null boundary and joint terms to the action and Gibbons-Hawking-York (GHY) terms. So,

$$\begin{aligned} I = & \frac{1}{16\pi G_N} \int_{\mathcal{M}} d^5x \sqrt{-g} \left[R - \frac{1}{2} (\partial\phi)^2 - V(\phi) \right] \\ & + \frac{1}{8\pi G_N} \int_{\mathcal{B}} d^4x \sqrt{|h|} K + \frac{1}{8\pi G_N} \int_{\Sigma} d^3x \sqrt{\sigma} \eta \\ & - \frac{1}{8\pi G_N} \int_{\mathcal{B}'} d\lambda d^3\theta \sqrt{\gamma} \kappa + \frac{1}{8\pi G_N} \int_{\Sigma'} d^3x \sqrt{\sigma} a. \end{aligned} \quad (4.10)$$

The affine parametrization could be chosen in a way that $\kappa = 0$ so to make the contribution of the null boundary vanish.

Now assuming $G_N = 1$ and $t_L = t_R = \frac{t}{2}$, we can divide the evolution of the black hole into two stages of the time before the critical time t_c , and after it. In the past critical time, the past null-boundary intersects the past-singularity and there is the GHY boundary term. After the critical time however, the two null boundaries from the left and right CFTs would intersect with

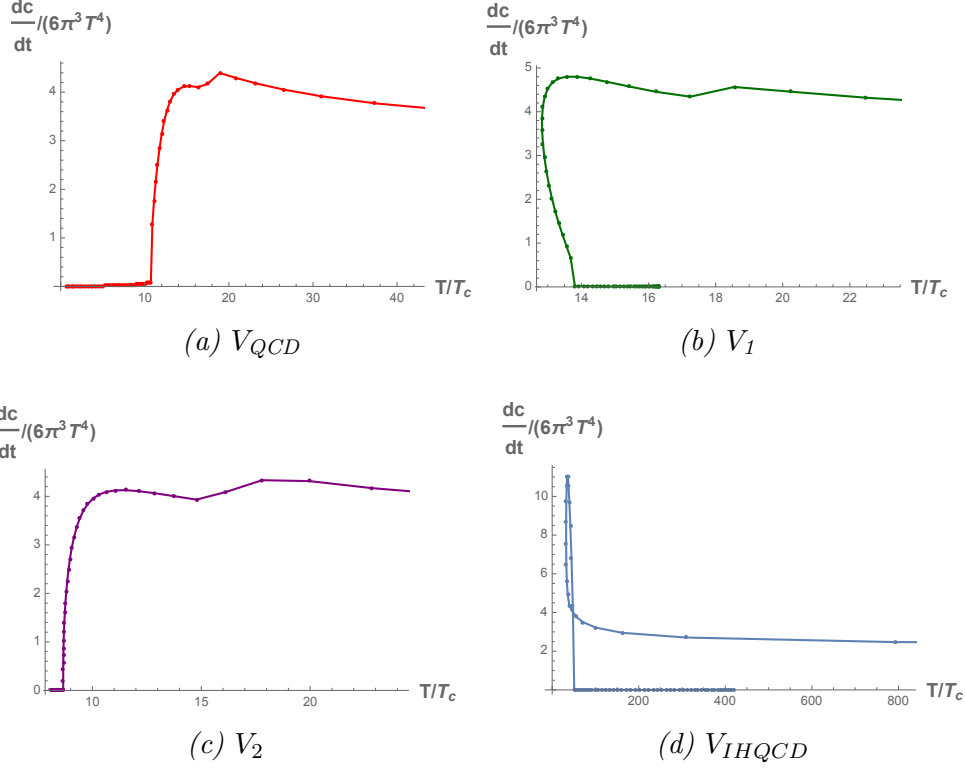


Figure 17: Phase transition of complexity growth rate versus temperature for four non-conformal cases.

each other and therefore there would be the contribution from the null joint term instead of the GHY term.

The critical time t_c could be found by

$$\begin{aligned} \frac{t_c}{2} - r^*(\infty) &= t - r^*(0), \\ -\frac{t_c}{2} + r^*(\infty) &= t + r^*(0), \end{aligned} \quad (4.11)$$

so

$$t_c = 2(r^*(\infty) - r^*(0)). \quad (4.12)$$

From Fig. 18, for a state at $r_R = t_L = \frac{t}{2} > \frac{t_c}{2}$, one gets

$$\begin{aligned} S_{bulk_I} &= \frac{2V_3}{3\pi G_N} \int_{r_H}^{r_{\max}} dr e^{4A+B} V(r) \left(\frac{t}{2} + r^*(0) - r^*(r) \right), \\ S_{bulk_{II}} &= \frac{4V_3}{3\pi G_N} \int_{\delta}^{r_H} dr e^{4A+B} V(r) (r^*(0) - r^*(r)), \\ S_{bulk_{III}} &= \frac{2V_3}{3\pi G_N} \int_{r_H}^{r_m} dr e^{4A+B} V(r) \left(-\frac{t}{2} + r^*(0) - r^*(r) \right), \end{aligned} \quad (4.13)$$

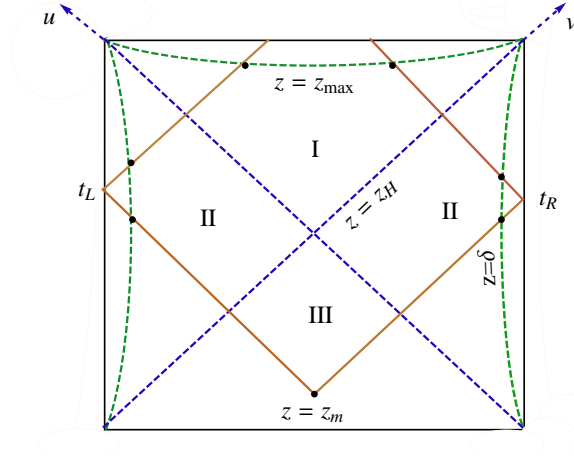


Figure 18: Penrose diagram for the black brane ansatz and the null boudaries.

so

$$S_{bulk} = \frac{4V_3}{3\pi G_N} \int_{\delta}^{r_{\max}} dr e^{4A+B} V(r) (r^*(0) - r^*(z)) + \frac{2V_3}{3\pi G_N} \int_{r_m}^{r_{\max}} dr e^{4A+B} V(r) \left(\frac{t}{2} - r^*(0) + r^*(r) \right). \quad (4.14)$$

Note that $r^*(r) = \int \frac{e^{B-A}}{h} dr$. Also the GHY boundary term at $r = r_{\max}$ would be

$$S_{\text{bound}} = \frac{V_3}{8\pi G_N} \left(\frac{t}{2} + r^*(0) - r^*(r_{\max}) \right) (e^{-4A-B} \partial_r (e^{8A} h))_{r=r_{\max}}. \quad (4.15)$$

Now, for considering the contribution of joint terms which occurs at $r = r_m$, we first take two normal vectors of the null boundaries,

$$k_1^a = \alpha \left(\frac{e^{-2A}}{h} (\partial_t)^a + e^{-A-B} (\partial_r)^a \right), \quad k_2^a = \beta \left(-\frac{e^{-2A}}{h} (\partial_t)^a + e^{-A-B} (\partial_r)^a \right). \quad (4.16)$$

Then, the joint action

$$S_{\text{joint}} = \frac{1}{8\pi G_N} \int d^d x \sqrt{\gamma} \log \left| \frac{k_1 \cdot k_2}{2} \right|, \quad (4.17)$$

would be

$$S_{\text{joint}} = \frac{V_3}{8\pi G_N} e^{3A(r_m)} (\log |e^{2A(r_m)}| - \log |h(r_m)|) + \frac{V_3}{8\pi G_N} e^{3A(r_m)} \log \alpha \beta. \quad (4.18)$$

In the above action, γ is the determinant of the induced metric on the joint point and α and β are two constants that appear because of the ambiguity in normalization of the null boundaries.

For removing the ambiguity, one can add a counter term which is in the following form

$$\frac{1}{8\pi G_N} \int d\lambda d^d x \sqrt{\gamma} \log \frac{\Theta}{d}, \quad (4.19)$$

where

$$\Theta = \frac{1}{\sqrt{\gamma}} \frac{\partial \sqrt{\gamma}}{\partial \lambda}. \quad (4.20)$$

Here, λ is the affine parameter for the null surface. For the null vector k_1 it would be

$$\frac{\partial r}{\partial \lambda} = \alpha e^{-A-B}. \quad (4.21)$$

For the null surface which is associated with k_1 , we have $\Theta = 3\alpha A' e^{-A-B}$, while for k_2 we get $\Theta = 3\beta A' e^{-A-B}$.

Then, the counter term would be

$$S_{ct} = -\frac{V_3}{4\pi G_N} \int_{\delta}^{r_m} dr 3A' e^{3A} \log(3A' e^{-A-B}) - \frac{V_3}{8\pi G_N} e^{3A(r_m)} \log \alpha \beta, \quad (4.22)$$

where the second term cancels the contribution from the normalization factors of 4.18.

So summing all the terms and taking the time derivative and also using $\frac{dr_m}{dt} = \frac{h(r_m(t))}{2} e^{A(r_m(t))-B(r_m(t))}$, we get

$$\begin{aligned} \frac{dS}{dt} / \frac{V_3}{\pi G_N} = & h(r_m) e^{A(r_m)-B(r_m)} \left(\frac{1}{3} e^{4A(r_m)+B(r_m)} V(r_m) r^*(r_m) \right. \\ & + \frac{3r_m}{8} e^{9r_m^2} (2 + 18r_m^2 - 3 \log(h(r_m))) - \frac{h'(r_m)}{6h(r_m)r_m} \Big) - \frac{3}{8} A'(r_m) e^{3A(r_m)} \log |3A'(r_m) e^{-A(r_m)-B(r_m)}| \\ & \left. + \frac{1}{3} \int_{r_m}^{r_{\max}} dz e^{4A+B} V(z) + \frac{1}{16} \left(e^{-4A-B} \partial_r (e^{8A} h) \right) \Big|_{r=r_{\max}} \right). \end{aligned}$$

The relationship between ϕ_m and t can be read numerically from the relation $t = 2(r^*(0) - r^*(r_m))$ (note $\phi = r$), and the plots for various ϕ_H for the different models of potential are shown in Fig. 19.

Interestingly these plots are very similar to the corresponding plots in [68]. In that work, the confining Einstein-Maxwell-dilaton model has been studied. Authors have found the relationship between the length of a strip ℓ of a subsystem which were used for calculating the entanglement entropy, versus z^* which is the turning point of the minimal area surface. Note that z^* actually corresponds to $\phi_m = r_m$ in our model. This actually would make sense as t and ℓ are directly connected. Note that when ϕ_m is smaller than ϕ_H , the relationship between t and ϕ_m is close to linear, but when ϕ_m reaches ϕ_H , then suddenly t blows up. These feature could be a universal

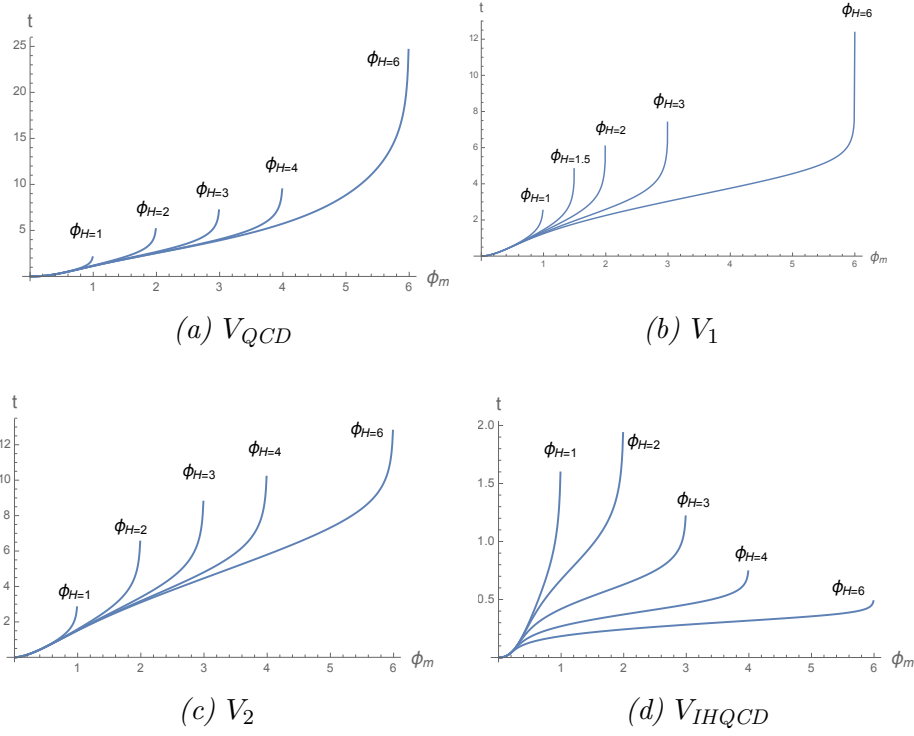


Figure 19: The relation between t and ϕ_m .

behavior of the confining models.

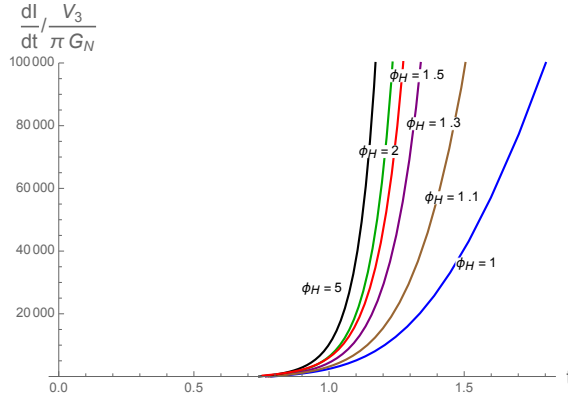


Figure 20: The rate of growth of complexity at early times for various black holes in the V_{QCD} model, with different ϕ_H , corresponding to different temperatures.

In Fig. 20, we present the full, time dependent, behavior of complexity growth rate coming from Eq. 4.23, for the case of V_{QCD} . For other potential models, the general behavior is qualitatively very similar. From this figure it is obvious that the Lloyd's bound would be violated at early times and it would be violated more strongly for black holes with higher temperatures.

However, one might expect that after this sudden increase, the rate of growth would decrease and then saturate at the Lloyd's bound. However, with only the terms that we considered here we did not observe such behavior. Therefore, considering some other counter terms should be

necessary and then adding them to the Eq. 4.23, could probably solve this issue and similar to other studies, the Lloyd's bound would be saturated from above. We leave finding such terms for these QCD models to future works.

In Fig. 21, we show the behavior of complexity growth rate $\frac{dC}{dt}$ versus ϕ_H for late times. One could see that at later times though, increasing ϕ_H would decrease the rate of growth of complexity. Also, the range of complexity growth for V_{IHQCD} is much bigger than the other ones. The phase transitions of this model for higher ϕ_H is also evident from the diagram.

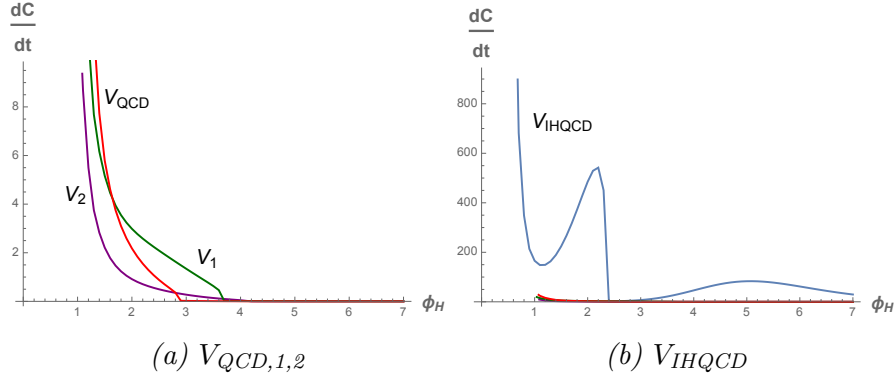


Figure 21: The relation between $\frac{dC}{dt}$ and ϕ_H .

By adding gauge fields to the action and using models such as the one in [69–71] and by doing the same calculations, one can similarly study the full time behavior of complexity growth rate for the *superconducting* phases and specifically during the phase transitions [72], which could have many practical applications in quantum information.

We are also interested to study the effects of hydrodynamics and non-hydrodynamic modes on the rate of growth of complexity and how these modes affect the different phase transitions during the complexity growth. We will discuss about it briefly in the following parts.

4.1 V_{QCD}

The parameters of this confining model have actually been chosen in a way to fit the data of the temperature dependence of the speed of sound which have been obtained from the lattice QCD.

With this potential we observe a crossover behavior at the zero baryon charge density. In this case, at lower temperatures, near the pseudocritical temperature $T = T_c$, there would be a rapid change in the large momentum dependence of the imaginary part of the hydrodynamic mode. As momentum increases, the imaginary part would flow to the minus infinity. This, as mentioned in [60], would point to a novel effect around $T = T_c$ in the sound channel where there would be a crossing between the hydrodynamic and non-hydrodynamic modes. It could be seen in Fig. 16a that actually at this point there is a sharp decrease in the speed of sound. Then from Fig. 22a, one can see that at this point, there would be a sharp increase in the rate of complexity growth.

Also, one could note that in all the figures, at high temperatures, the speed of sound would reach to $1/3$, which is the expected value for the conformal case or plasmas with a very high T .

In the higher temperature regions, where the results match with the conformal case, the non-hydrodynamic modes are actually the most effective ones, while in the lower temperature points, the hydrodynamic modes play the most important role. Also, it is worth to notice that the hydrodynamic modes (at lower temperature, and around $T = T_c$) are much more affected by the “ultra locality property” of the system as it was mentioned in [73]. This could actually greatly affect the complexity growth rate of the QCD systems as we have observed.

4.2 V_1

This model is actually the most interesting one as it has some distinctive features. The parameters for this model have been constructed in a way to generate a first order phase transition. In this case one could observe instability or spinodal region for a certain temperature range where this behavior could also be seen from the phase diagrams of entropy, complexity growth and specially the diagram for the speed of sound.

In fact, the first order phase transition appears in two different scenarios [60]. One is similar to the Hawking-Page scenario where the transition is between a black hole and a thermal gas. The other one is between two black holes with different sizes. In this case for our V_1 model, the first order phase transition is actually between two black holes [74]. The fact that both of these cases could happen is due to the functional dependence of the dilaton field potential on the radial distance in the deep infrared region. Another distinctive feature is the existence of non-propagating sound mode in the very low temperature which also shows its effects on the complexity growth rate phase diagram.

The most important feature in this model though, is the presence of the *spinodal* region which has been studied in the nuclear physics in the context of spinodal multifragmentation [75]. One can also see from the diagram of the speed of sound (as $c_s^2 < 0$), there exist a dynamical instability during phase transition which are caused from the bubble formation in this region.

The same kind of behavior has also been observed in gravitational studies of black strings and p-branes in the context of Gregory and Laflamme instability, [76]. Note that in this case the hydrodynamical modes are purely imaginary and this shows its effect on the complexity growth rate as well. It could be seen from the fact that, unlike the cross over and second order phase transition where the slopes of $\frac{dC}{dt}$ versus T/T_c are positive, in this case the slope of complexity growth during the phase transition is actually negative. This behavior could be a universal property of complexity for the regions with “*hydrodynamical instabilities*” with purely imaginary mode.

4.3 V_2

In this model at a critical temperature $T = T_c$, the speed of sound would vanish which could be checked from Fig. 16c. Also, near the critical temperature the entropy behaves as

$$s(T) \sim s_0 + s_1 (T/T_c - 1)^{1-\alpha}, \quad (4.23)$$

where according to [58], the constant in the power should be $\alpha = 2/3$. As the complexity growth rate phase diagram is very similar to the entropy diagram, we expect that this relation could approximately describe the complexity growth rate behavior near critical temperature as well.

Notice that in all the diagrams of entropy, complexity growth rate and speed of sound, (Fig 22) and also the time dependences of ϕ_m (Fig 19), the behavior for the V_2 case is very similar to V_{QCD} case. The main difference is that V_2 is actually in the back of V_{QCD} .

As mentioned in [60], the generic temperature dependence of the frequencies of the quasi normal modes are also very similar to those of the crossover case. This, therefore, would make all the corresponding quantities of these two models act similar to each other around the critical temperature.

Actually, the hydrodynamic description of the system would break down at smaller momenta scales, [60]. This would make the critical temperature of V_2 lower than the crossover case. For the higher temperatures, all of these models including V_2 would behave the same way and similar to the conformal case.

In order to get some more detailed results about the relationship between the different characteristics of the model and the behavior of the growth of complexity, the numerical data points for the plot of complexity could be increased. This would then increase the calculation time dramatically.

4.4 V_{IHQCD}

The improved holographic QCD model is very unique compare to other models and acts substantially different from the other ones. It has been constructed in order to best model the dynamical properties of QCD, specifically the asymptotic freedom, color confinement and to get a more realistic value for the bulk viscosity. In this model there is a first order phase transition, but between a black hole and a thermal gas or a vacuum confining geometry, similar to Hawking-Page phase transition. This fact could actually explain the sharp drop in the phase diagram of the complexity growth rate of this model, check Fig. 17d.

The exact critical temperature were the first order phase transition would occur would be very difficult to determine for this case as there are several solutions with instabilities and also the temperature of the reference geometry which is the thermal gas would be infinite. However, from the diagrams, the phase transition point has a very distinct behavior since at that point

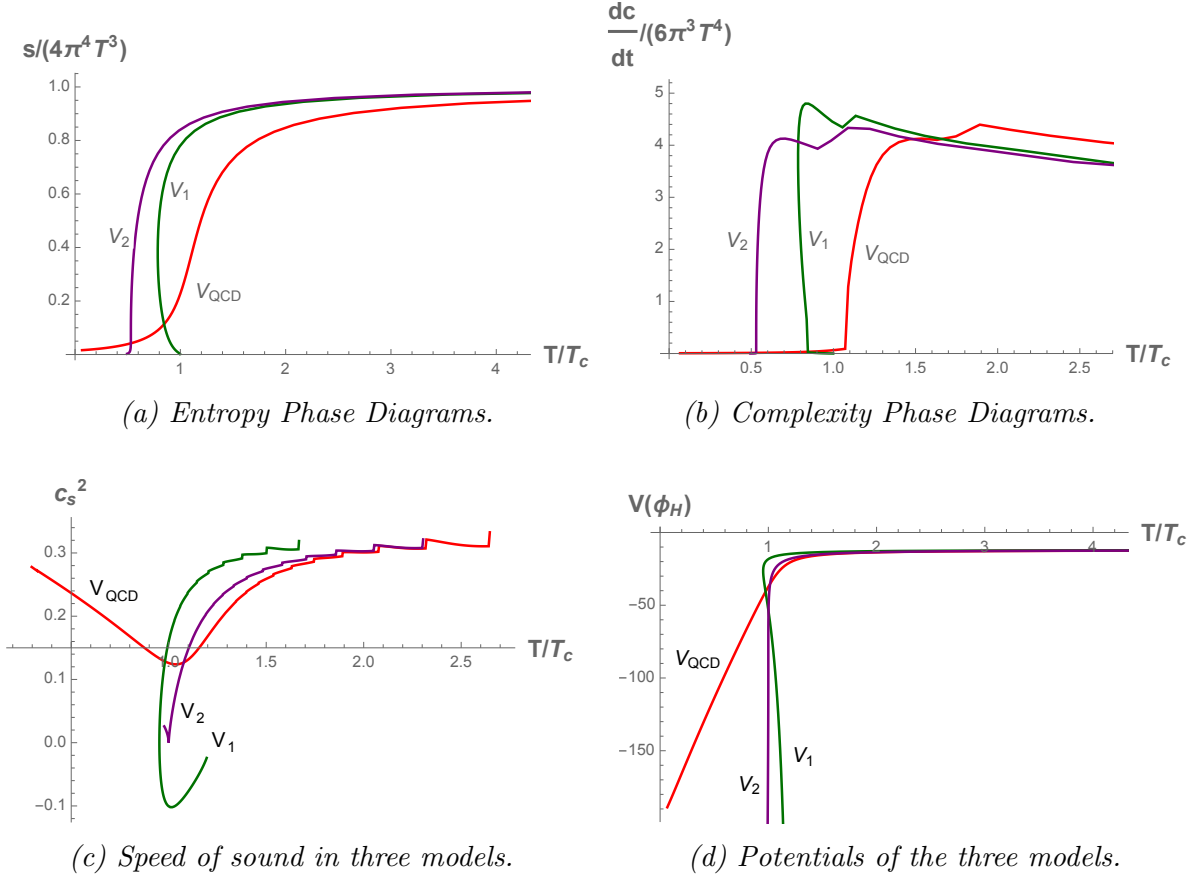


Figure 22: Comparing different quantities for three models of QCD.

the geometry changes dramatically, which is also apparent in the diagrams of speed of sound and specifically complexity growth rate.

From these diagrams one could actually detect two characteristic temperatures which are very close to each other. As mentioned in [60], for the temperatures between these two and for low momenta, the lowest lying excitation modes become purely imaginary which leads to ultralocality violation in this section. This greatly impacts the first phase of the complexity growth rate. Then notice that at $T = T_m$, for some modes, the hydrodynamic mode and the first non-hydrodynamic mode would have the same dispersion relation. At a critical temperature T_c , a bit higher than T_m , a transition which changes the geometry substantially would take place. This would cause the rapid increase and then the falling down in the plot of complexity growth rate.

The plot shown in Fig. 16d is actually for the unstable smaller black hole. The stable case which models the behavior of the pure glue system [77] is not shown here and we leave it for the future studies. The plot of speed of sound shown here still could communicate the existence of spinodal instability and therefore the bubble formation. Specifically for the small black hole region the speed of sound is anomalously large and then become superluminal violating the causality. This actually points out to a “dynamical” instability which is different from the “spinoidal case” seen before. This difference of behavior could also be detected from the behavior of normal modes [60]

and specifically from the complexity growth rate behavior shown in Figs. 15d, 16d, 17d and even Fig. 21.

By studying the poles of Green's functions, the behavior of hydrodynamic and non-hydrodynamic modes have been discussed in more details in [60]. It has been shown that the modes would be degenerated close to the minimal black hole temperature and there would exist a region of temperatures where the non-hydrodynamical modes would be unstable.

In [60], it has been pointed out that a small gap between the degrees of freedom at low momentums would exist. The non-hydrodynamical modes show *ultralocal* properties as they have weak dependence on the momentum scale. It would be interesting to study the effects of such non local modes on the behavior of complexity growth rates. Also, a more careful study of the behavior of complexity growth rate close to the mode gap between the two solutions would be very interesting.

Finally, it is worth to note that as the modes of this system would match the results from the holographic dual of superfluid systems, [60, 78], one would expect that the behavior of growth of quantum complexity shown in Fig. 17d, would actually match the behavior of growth of complexity in superfluid systems which again might be able to be tested experimentally.

5 Discussion

In this work we showed the relationship between different field potentials and complexity growth rate behavior in several models such as charged dilaton, Born-Infeld and dyonic black hole. We conjectured that it would be a universal feature of complexity that, for potential wells, the complexity growth rate would be higher and for parameters of the model which there is a steep potential barrier, the complexity growth rate would decrease to zero. This could indicate that quantum fluctuations such as tunneling would be the main source of complexity growth rate after thermalization point.

Also, we studied the complexity growth rates during different phase transitions. First, for the dyonic black hole, we studied the full time behavior. Similar to other studies, we found that the Lloyd's bound would be violated at early times but then at later times it would be saturated from above. Changing the charges of the black hole could reveal a second order phase transition in the complexity growth rate which is similar to the phase transition of the van der Waals fluid. For very big charges, the complexity growth rate would diverge as we have expected, since at those ranges of charge the black hole would be unstable. Therefore, we found that complexity growth rate could be a very suitable probe to catch different phase transitions and instabilities.

To further explore this point, we considered the complexity growth rate of AdS soliton black holes which for the first time has been studied in [31]. We compared the behavior of complexity growth rates in AdS soliton and pure AdS case, the potential behavior in the AdS soliton with its tachyonic condensation, and also we compared the Schwinger phase diagrams and again we observed strong correlations.

Finally, for the main part of this work, we studied the Gubser model of QCD [57, 58] which by tuning the parameters of the potential for the V_{QCD} , V_1 , V_2 cases, the crossover, first and second order phase transitions could be generated. We also studied the improved holographic QCD potential model, V_{HQCD} which improves modeling the dynamical properties. Solving for the entropies, complexity rates, speed of sounds and potentials numerically, we observed similarities in their behavior near the phase transition points in each model. By considering the crossings between hydrodynamic and non-hydrodynamic modes, we then explained different features of complexity growth rates and the phase diagrams.

For the full, time dependent phase diagrams, however, we showed that additional counter terms in the action for this QCD model would be needed to produce the desired behavior considering the Lloyd's bound.

For the future works, one could make the argument of relationship between complexity growth rate and particle creation and annihilation rates more precise. For doing that, one could imagine Schwinger mechanism as the motion in the space of unitary operators and then using the intuition from [27] and [28], calculate how much pair creation or vacuum quantum fluctuations would increase the distance between the initial state at t_0 and the state at later times after only one pair creation. Holographic methods of considering an open string, writing the Nambu-Goto action and the induced metric on the string worldsheet, and then adding proper boundary and joint terms for calculating the action could be used to solve this problem. The first few steps have been taken in the final part of [34]. The main challenge that one would face is determining the correct Wheeler-DeWitt. Solving these issues and comparing with the results from field theory methods such as the one in [30], one then could check if actually the creation of these particles would move on the optimal path of increasing the computational complexity which would be a very interesting problem.

As a side note, in [37, 56] for different backgrounds, the decay rate is found to increase with the magnetic field parallel to the electric field, while it decreases with the magnetic field perpendicular to the electric field which seems to be a universal feature of Schwinger effect. One then could check how in the presence of electric and magnetic fields for two setups of magnetic field parallel and perpendicular to the electric field, the complexity growth rates would be different. Comparing the results could strengthen our conjecture then.

The relationship between “shear viscosity” of black holes and the rate of complexity growth rate specially around the critical temperature could also be studied. This specifically would be an interesting problem with practical applications. For instance as it has been suggested in [79], in quark-gluon plasmas, there would be a sharp rise in the bulk viscosity near the deconfinement transition which actually points to the “soft statistically hadronization” of the plasma. So, it would be interesting to study the complexity growth rate at this point and depict the relationship between complexity and shear or bulk viscosity of black holes and the corresponding QCD phases.

We hope to study these questions in the future works.

Acknowledgement

I thank Hesam Soltanpanahi and Saeedeh Sadeghian for useful discussions.

References

- [1] S. Ryu and T. Takayanagi, *Holographic derivation of entanglement entropy from AdS/CFT*, *Phys. Rev. Lett.* **96** (2006) 181602, [[hep-th/0603001](#)].
- [2] L. Susskind, *Computational Complexity and Black Hole Horizons*, *Fortsch. Phys.* **64** (2016) 44–48, [[arXiv:1403.5695](#)]. [*Fortsch. Phys.* 64,24(2016)].
- [3] A. R. Brown, D. A. Roberts, L. Susskind, B. Swingle, and Y. Zhao, *Complexity, action, and black holes*, *Phys. Rev.* **D93** (2016), no. 8 086006, [[arXiv:1512.04993](#)].
- [4] M. Alishahiha, *Holographic Complexity*, *Phys. Rev.* **D92** (2015), no. 12 126009, [[arXiv:1509.06614](#)].
- [5] A. R. Brown, D. A. Roberts, L. Susskind, B. Swingle, and Y. Zhao, *Holographic Complexity Equals Bulk Action?*, *Phys. Rev. Lett.* **116** (2016), no. 19 191301, [[arXiv:1509.07876](#)].
- [6] R.-G. Cai, M. Sasaki, and S.-J. Wang, *Action growth of charged black holes with a single horizon*, *Phys. Rev.* **D95** (2017), no. 12 124002, [[arXiv:1702.06766](#)].
- [7] A. Bhattacharyya, P. Caputa, S. R. Das, N. Kundu, M. Miyaji, and T. Takayanagi, *Path-Integral Complexity for Perturbed CFTs*, *JHEP* **07** (2018) 086, [[arXiv:1804.01999](#)].
- [8] D. Carmi, S. Chapman, H. Marrochio, R. C. Myers, and S. Sugishita, *On the Time Dependence of Holographic Complexity*, *JHEP* **11** (2017) 188, [[arXiv:1709.10184](#)].
- [9] M. Ghodrati, *Complexity growth in massive gravity theories, the effects of chirality, and more*, *Phys. Rev.* **D96** (2017), no. 10 106020, [[arXiv:1708.07981](#)].
- [10] R. Auzzi, S. Baiguera, and G. Nardelli, *Volume and complexity for warped AdS black holes*, *JHEP* **06** (2018) 063, [[arXiv:1804.07521](#)].
- [11] R. Auzzi, S. Baiguera, M. Grassi, G. Nardelli, and N. Zenoni, *Complexity and action for warped AdS black holes*, [arXiv:1806.06216](#).
- [12] R. Abt, J. Erdmenger, M. Gerbershagen, C. M. Melby-Thompson, and C. Northe, *Holographic Subregion Complexity from Kinematic Space*, [arXiv:1805.10298](#).
- [13] W. Cottrell and M. Montero, *Complexity is simple!*, *JHEP* **02** (2018) 039, [[arXiv:1710.01175](#)].

- [14] C. A. Agn, M. Headrick, and B. Swingle, *Subsystem Complexity and Holography*, [arXiv:1804.01561](#).
- [15] B. Swingle and Y. Wang, *Holographic Complexity of Einstein-Maxwell-Dilaton Gravity*, [arXiv:1712.09826](#).
- [16] K. Hashimoto, N. Iizuka, and S. Sugishita, *Thoughts on Holographic Complexity and its Basis-dependence*, *Phys. Rev.* **D98** (2018), no. 4 046002, [[arXiv:1805.04226](#)].
- [17] J. L. F. Barbon and J. Martin-Garcia, *Terminal Holographic Complexity*, *JHEP* **06** (2018) 132, [[arXiv:1805.05291](#)].
- [18] D. Ageev, I. Aref 'eva, A. Bagrov, and M. I. Katsnelson, *Holographic local quench and effective complexity*, [arXiv:1803.11162](#).
- [19] L.-P. Du, S.-F. Wu, and H.-B. Zeng, *Holographic complexity of the disk subregion in (2+1)-dimensional gapped systems*, [arXiv:1803.08627](#).
- [20] B. Chen, W.-M. Li, R.-Q. Yang, C.-Y. Zhang, and S.-J. Zhang, *Holographic subregion complexity under a thermal quench*, *JHEP* **07** (2018) 034, [[arXiv:1803.06680](#)].
- [21] A. Ovgi and K. Jusufi, *Complexity growth rates for AdS black holes with dyonic/ nonlinear charge/ stringy hair/ topological defects*, [arXiv:1801.09615](#).
- [22] Z. Fu, A. Maloney, D. Marolf, H. Maxfield, and Z. Wang, *Holographic complexity is nonlocal*, *JHEP* **02** (2018) 072, [[arXiv:1801.01137](#)].
- [23] M. Flory and N. Miekley, *Complexity change under conformal transformations in AdS_3/CFT_2* , [arXiv:1806.08376](#).
- [24] P. Caputa and J. M. Magan, *Quantum Computation as Gravity*, [arXiv:1807.04422](#).
- [25] P. Caputa, N. Kundu, M. Miyaji, T. Takayanagi, and K. Watanabe, *Liouville Action as Path-Integral Complexity: From Continuous Tensor Networks to AdS/CFT*, *JHEP* **11** (2017) 097, [[arXiv:1706.07056](#)].
- [26] R. Abt, J. Erdmenger, H. Hinrichsen, C. M. Melby-Thompson, R. Meyer, C. Northe, and I. A. Reyes, *Topological Complexity in AdS_3/CFT_2* , *Fortsch. Phys.* **66** (2018), no. 6 1800034, [[arXiv:1710.01327](#)].
- [27] R. A. Jefferson and R. C. Myers, *Circuit complexity in quantum field theory*, *JHEP* **10** (2017) 107, [[arXiv:1707.08570](#)].
- [28] S. Chapman, M. P. Heller, H. Marrochio, and F. Pastawski, *Towards Complexity for Quantum Field Theory States*, [arXiv:1707.08582](#).

- [29] R. Khan, C. Krishnan, and S. Sharma, *Circuit Complexity in Fermionic Field Theory*, [arXiv:1801.07620](#).
- [30] L. Hackl and R. C. Myers, *Circuit complexity for free fermions*, *JHEP* **07** (2018) 139, [[arXiv:1803.10638](#)]. [Physics2018,139(2018)].
- [31] A. P. Reynolds and S. F. Ross, *Complexity of the AdS Soliton*, [arXiv:1712.03732](#).
- [32] M. Guo, J. Hernandez, R. C. Myers, and S.-M. Ruan, *Circuit Complexity for Coherent States*, [arXiv:1807.07677](#).
- [33] A. Bhattacharyya, A. Shekar, and A. Sinha, *Circuit complexity in interacting QFTs and RG flows*, [arXiv:1808.03105](#).
- [34] J. de Boer, E. Llabrs, J. F. Pedraza, and D. Vegh, *Chaotic strings in AdS/CFT*, [arXiv:1709.01052](#).
- [35] M. Ghodrati, *Hyperscaling Violating Solution in Coupled Dilaton-Squared Curvature Gravity*, *Phys. Rev.* **D90** (2014), no. 4 044055, [[arXiv:1404.5399](#)].
- [36] S.-J. Zhang, *Complexity and phase transitions in a holographic QCD model*, [arXiv:1712.07583](#).
- [37] M. Ghodrati, *Schwinger Effect and Entanglement Entropy in Confining Geometries*, *Phys. Rev.* **D92** (2015), no. 6 065015, [[arXiv:1506.08557](#)].
- [38] M. Kord Zangeneh, Y. C. Ong, and B. Wang, *Entanglement Entropy and Complexity for One-Dimensional Holographic Superconductors*, *Phys. Lett.* **B771** (2017) 235–241, [[arXiv:1704.00557](#)].
- [39] M. Ghodrati and A. Naseh, *Phase transitions in Bergshoeff-Hohm-Townsend massive gravity*, *Class. Quant. Grav.* **34** (2017), no. 7 075009, [[arXiv:1601.04403](#)].
- [40] H. A. Camargo, P. Caputa, D. Das, M. P. Heller, and R. Jefferson, *Complexity as a novel probe of quantum quenches: universal scalings and purifications*, [arXiv:1807.07075](#).
- [41] M. Ghodrati, *Beyond AdS Space-times, New Holographic Correspondences and Applications*. PhD thesis, Michigan U., MCTP, 2016. [arXiv:1609.04168](#).
- [42] M. Ghodrati, K. Hajian, and M. R. Setare, *Revisiting Conserved Charges in Higher Curvature Gravitational Theories*, *Eur. Phys. J.* **C76** (2016), no. 12 701, [[arXiv:1606.04353](#)].
- [43] M. Alishahiha, A. Faraji Astaneh, M. R. Mohammadi Mozaffar, and A. Mollabashi, *Complexity Growth with Lifshitz Scaling and Hyperscaling Violation*, [arXiv:1802.06740](#).

- [44] C. J. Gao and S. N. Zhang, *Dilaton black holes in de Sitter or Anti-de Sitter universe*, *Phys. Rev. D* **70** (2004) 124019, [[hep-th/0411104](#)].
- [45] Y.-S. An and R.-H. Peng, *The effect of Dilaton on the holographic complexity growth*, [arXiv:1801.03638](#).
- [46] S. Dutta, A. Jain, and R. Soni, *Dyonic Black Hole and Holography*, *JHEP* **12** (2013) 060, [[arXiv:1310.1748](#)].
- [47] S. Chapman, H. Marrochio, and R. C. Myers, *Holographic complexity in Vaidya spacetimes. Part I*, *JHEP* **06** (2018) 046, [[arXiv:1804.07410](#)].
- [48] S. Chapman, H. Marrochio, and R. C. Myers, *Holographic Complexity in Vaidya Spacetimes II*, *JHEP* **06** (2018) 114, [[arXiv:1805.07262](#)].
- [49] A. Chamblin, R. Emparan, C. V. Johnson, and R. C. Myers, *Charged AdS black holes and catastrophic holography*, *Phys. Rev. D* **60** (1999) 064018, [[hep-th/9902170](#)].
- [50] H. Xu, *Entanglement growth during Van der Waals like phase transition*, *Phys. Lett. B* **772** (2017) 517–522, [[arXiv:1705.02604](#)].
- [51] T. Nishioka and T. Takayanagi, *AdS Bubbles, Entropy and Closed String Tachyons*, *JHEP* **01** (2007) 090, [[hep-th/0611035](#)].
- [52] G. T. Horowitz and E. Silverstein, *The Inside story: Quasilocal tachyons and black holes*, *Phys. Rev. D* **73** (2006) 064016, [[hep-th/0601032](#)].
- [53] G. T. Horowitz and R. C. Myers, *The AdS / CFT correspondence and a new positive energy conjecture for general relativity*, *Phys. Rev. D* **59** (1998) 026005, [[hep-th/9808079](#)].
- [54] D. Ghoshal and A. Sen, *Tachyon condensation and brane descent relations in p-adic string theory*, *Nucl. Phys. B* **584** (2000) 300–312, [[hep-th/0003278](#)].
- [55] F. M. Haehl, *The Schwarzschild-Black String AdS Soliton: Instability and Holographic Heat Transport*, *Class. Quant. Grav.* **30** (2013) 055002, [[arXiv:1210.5763](#)].
- [56] K. Hashimoto, T. Oka, and A. Sonoda, *Electromagnetic instability in holographic QCD*, *JHEP* **06** (2015) 001, [[arXiv:1412.4254](#)].
- [57] S. S. Gubser, A. Nellore, S. S. Pufu, and F. D. Rocha, *Thermodynamics and bulk viscosity of approximate black hole duals to finite temperature quantum chromodynamics*, *Phys. Rev. Lett.* **101** (2008) 131601, [[arXiv:0804.1950](#)].
- [58] S. S. Gubser and A. Nellore, *Mimicking the QCD equation of state with a dual black hole*, *Phys. Rev. D* **78** (2008) 086007, [[arXiv:0804.0434](#)].

- [59] R. A. Janik, J. Jankowski, and H. Soltanpanahi, *Nonequilibrium Dynamics and Phase Transitions in Holographic Models*, *Phys. Rev. Lett.* **117** (2016), no. 9 091603, [[arXiv:1512.06871](#)].
- [60] R. A. Janik, J. Jankowski, and H. Soltanpanahi, *Quasinormal modes and the phase structure of strongly coupled matter*, *JHEP* **06** (2016) 047, [[arXiv:1603.05950](#)].
- [61] R. A. Janik, J. Jankowski, and H. Soltanpanahi, *Real-Time dynamics and phase separation in a holographic first order phase transition*, *Phys. Rev. Lett.* **119** (2017), no. 26 261601, [[arXiv:1704.05387](#)].
- [62] R. Zllner and B. Kampfer, *Phase structures emerging from holography with Einstein gravity - dilaton models at finite temperature*, [arXiv:1807.04260](#).
- [63] S.-J. Zhang, *Holographic entanglement entropy close to crossover/phase transition in strongly coupled systems*, *Nucl. Phys.* **B916** (2017) 304–319, [[arXiv:1608.03072](#)].
- [64] D. Stanford and L. Susskind, *Complexity and Shock Wave Geometries*, *Phys. Rev.* **D90** (2014), no. 12 126007, [[arXiv:1406.2678](#)].
- [65] L. Susskind, *Entanglement is not enough*, *Fortsch. Phys.* **64** (2016) 49–71, [[arXiv:1411.0690](#)].
- [66] A. Anabalon, T. Andrade, D. Astefanesei, and R. Mann, *Universal Formula for the Holographic Speed of Sound*, *Phys. Lett.* **B781** (2018) 547–552, [[arXiv:1702.00017](#)].
- [67] L. Lehner, R. C. Myers, E. Poisson, and R. D. Sorkin, *Gravitational action with null boundaries*, *Phys. Rev.* **D94** (2016), no. 8 084046, [[arXiv:1609.00207](#)].
- [68] D. Dudal and S. Mahapatra, *Interplay between the holographic QCD phase diagram and entanglement entropy*, *JHEP* **07** (2018) 120, [[arXiv:1805.02938](#)].
- [69] S. S. Gubser, *Phase transitions near black hole horizons*, *Class. Quant. Grav.* **22** (2005) 5121–5144, [[hep-th/0505189](#)].
- [70] S. S. Gubser, *Breaking an Abelian gauge symmetry near a black hole horizon*, *Phys. Rev.* **D78** (2008) 065034, [[arXiv:0801.2977](#)].
- [71] C. P. Herzog, *Lectures on Holographic Superfluidity and Superconductivity*, *J. Phys.* **A42** (2009) 343001, [[arXiv:0904.1975](#)].
- [72] D. Momeni, S. A. H. Mansoori, and R. Myrzakulov, *Holographic Complexity in Gauge/String Superconductors*, *Phys. Lett.* **B756** (2016) 354–357, [[arXiv:1601.03011](#)].

- [73] R. A. Janik, G. Plewa, H. Soltanpanahi, and M. Spalinski, *Linearized nonequilibrium dynamics in nonconformal plasma*, *Phys. Rev.* **D91** (2015), no. 12 126013, [[arXiv:1503.07149](#)].
- [74] U. Gursoy, E. Kiritsis, L. Mazzanti, and F. Nitti, *Holography and Thermodynamics of 5D Dilaton-gravity*, *JHEP* **05** (2009) 033, [[arXiv:0812.0792](#)].
- [75] P. Chomaz, M. Colonna, and J. Randrup, *Nuclear spinodal fragmentation*, *Phys. Rept.* **389** (2004) 263–440.
- [76] R. Gregory and R. Laflamme, *Black strings and p-branes are unstable*, *Phys. Rev. Lett.* **70** (1993) 2837–2840, [[hep-th/9301052](#)].
- [77] G. Boyd, J. Engels, F. Karsch, E. Laermann, C. Legeland, M. Lutgemeier, and B. Petersson, *Thermodynamics of $SU(3)$ lattice gauge theory*, *Nucl. Phys.* **B469** (1996) 419–444, [[hep-lat/9602007](#)].
- [78] I. Amado, M. Kaminski, and K. Landsteiner, *Hydrodynamics of Holographic Superconductors*, *JHEP* **05** (2009) 021, [[arXiv:0903.2209](#)].
- [79] F. Karsch, D. Kharzeev, and K. Tuchin, *Universal properties of bulk viscosity near the QCD phase transition*, *Phys. Lett.* **B663** (2008) 217–221, [[arXiv:0711.0914](#)].